SUPPORTING INFORMATION

to

Mechanism of Strand-Specific Smooth Muscle α-Actin Enhancer Interaction by Purine-Rich Element Binding Protein B (Purβ)[†]

Jon E. Ramsey[‡⊥] and Robert J. Kelm, Jr.[‡§‖*]

Departments of [‡]Biochemistry and [§]Medicine, [‖]Cardiovascular Research Institute, University of Vermont College of Medicine, Burlington, Vermont 05405

[*] To whom correspondence should be addressed: Robert J. Kelm, Jr., Ph.D., Department of Medicine, University of Vermont, Colchester Research Facility, 208 South Park Drive, Colchester, VT 05446. Tel: 802-656-0329, Fax: 802-656-8969, Email: robert.kelm@uvm.edu

[⊥] Present Address: Department of Biochemistry and Molecular Biology, Mail Stop 3030, University of Kansas Medical Center, 3901 Rainbow Blvd., Kansas City, KS 66160.

SUPPORTING MATERIALS AND METHODS

Recombinant Purα, fibroblast nuclear extracts, and Pur antibodies. Recombinant Purα was expressed as an amino-terminal hexahistidine-tagged fusion protein in *E. coli* and purified as described previously (*1, 2*). Nuclear extracts from AKR-2B mouse embryonic fibroblasts were prepared from cell monolayers cultured under exponential growth conditions (*3*). Protein concentrations were assessed by bicinchoninic acid assay (Sigma-Aldrich) using high purity BSA (Boehringer-Mannheim) as a standard. The specificity of rabbit polyclonal antibodies against carboxy-terminal sequences in mouse Purα (anti-Purα 291-313) or Purβ (anti-Purβ 302-324) was evaluated and documented previously (*4*).

Colorimetric ssDNA-Binding Immunoassay. Biotinylated single-stranded DNA probe was immobilized on streptavidin-coated microtiter wells (Streptawells™, Roche Applied Science) by application of 100 μL/well of 1.0 nM PE32-bF in buffer consisting of 20 mM HEPES pH 7.5, 150 mM NaCl, 1.5 mM $MgCl_2$ at 20 ± 1°C for 1 h with moderate shaking. Solutions were removed and wells were rinsed three times with 300 μL of wash buffer consisting of 20 mM HEPES pH 7.5, 150 mM NaCl, 1.5 mM $MgCl_2$, 0.05% (v/v) Tween 20. This was followed by application of 250 μL/well of blocking buffer consisting of 20 mM HEPES pH 7.5, 150 mM NaCl, 1.5 mM $MgCl_2$, 20 mg/ml BSA at 20 ± 1°C for 1 h with moderate shaking. Wells were again rinsed three times with 300 μL of wash buffer. Solutions containing 1.0 nM N-HisPurβ and selected concentrations of competing oligonucleotides in binding buffer consisting of 50 mM Tris-HCl pH 7.5, 100 mM KCl, 0.5 mM dithiothreitol, 2 μg/ml dT_{32}, 50 μg/ml BSA were added at 100 μL/well and incubated at least 12 h at 4°C. After overnight incubation, wells were triply washed as above. Solid-phase N-HisPurβ nucleoprotein complexes were detected by addition of 100 μL of primary antibody solution containing 1.0 μg/ml rabbit anti-Purβ 302-324 in antibody

buffer consisting of 20 mM HEPES pH 7.5, 150 mM NaCl, 1.5 mM $MgCl_2$, 0.05% Tween 20, 2 mg/ml BSA for 1 h at 20 ± 1°C. This was followed by triplicate washing and addition of 100 μL of secondary antibody solution containing 40 ng/mL goat anti-rabbit horseradish peroxidase conjugate (Santa Cruz Biotechnologies) in antibody buffer to each well and incubation for 1 h at 20 ± 1°C. Wells were again washed three times and 100 μL of 2,2'-azino-bis(3-ethylbenzthiazoline-6-sulfonic acid) substrate solution (ABTS, Chemicon) was added. After satisfactory color development by incubation at room temperature for ~5 min, 100 μL of 1% (w/v) sodium dodecylsulfate was added and solution absorbance readings at 405 nm were obtained with a microplate reader. The sequence and corresponding promoter location of all SMαA-derived oligonucleotide competitors employed in this assay are listed in Table S1.

Analysis of Flourescence Anistropy Data to Determine Purβ:PE32-F Stoichiometry. For the completely cooperative reaction, $nP + D \rightleftarrows P_nD$, where P is the protein ligand, D is the DNA lattice and n is the stoichiometry of the terminal complex, the constant K_r can be defined as:

$$K_r = \frac{[P][D]}{[P_nD]} \qquad \text{(S1)}$$

Note that K_r is not a true equilibrium constant in cases where n is greater than unity. Substituting terms that take into account the law of mass action, K_r can be written as:

$$K_r = \frac{([P_t] - n[P_nD])([D_t]-[P_nD])}{[P_nD]} \qquad \text{(S2)}$$

where $[P_t]$ and $[D_t]$ represent the total concentrations of protein and DNA, respectively. Solving for $[P_nD]$ gives the following quadratic equation.

$$[P_nD] = \frac{([P_t] + n[D_t] + K_r) \pm (([P_t] + n[D_t] + K_r)^2 - 4n[P_t][D_t])^{1/2}}{2n} \qquad \text{(S3)}$$

For a mixture of molecular species with different anisotropies (but with the same fluorescence intensities), the measurable anisotropy of the solution (r_{obs}) is the sum of the mole fractions of the individual species multiplied by their inherent anisotropic values (*5, 6*):

$$r_{obs} = f_1 r_1 + f_2 r_2 + \ldots + f_i r_i \qquad \text{(S4)}$$

where f_i is the mole fraction (and quantum yield) and r_i is the anisotropy of the ith species. Equation S4 can be rearranged and expressed in terms of fraction bound, f_B:

$$f_B = \frac{[P_n D]}{[D_t]} = \frac{(r_{obs} - r_f)}{(r_b - r_f)} \qquad \text{(S5)}$$

where r_b and r_f is the anisotropy of the bound and free species, respectively. Substituting equation S5 into equation S3 and applying terms that accommodate nonspecific binding gives equation S6:

$$r_{obs} = b(r_b - r_f)\frac{1}{[D_t]}\left\{\frac{(R_{P/D}[D_t] + n[D_t] + K_r) \pm ((R_{P/D}[D_t] + n[D_t] + K_r)^2 - 4nR_{P/D}[D_t]^2)^{1/2}}{2n}\right\} + r_f + mR_{P/D}[D_t] \qquad \text{(S6)}$$

where $R_{P/D}$ is the molar ratio, $[P_t]/[D_t]$, and b and m are non-specificity terms that permit both the fluctuation of the equivalence saturation point and the slope of the plateau region due to non-specific binding, respectively. Obtained anisotropy values, r_{obs}, for titrations of N-HisPurβ against fixed concentrations of PE32-F-3FLC were plotted against known values of $R_{P/D}$, and fit to Equation S6 to obtain best-fit values of n using Prism 5 software (GraphPad Software, Inc.).

EMSA with Nuclear Extracts and Antibodies. Purified recombinant proteins and crude nuclear extracts were diluted in EMSA binding buffer (main text) supplemented with 0.5 mM EDTA to limit nuclease activity in the cell extracts. Radiolabeled ssDNA probe (PE32-F*) was added to a final concentration of 1.0 nM. Binding reactions were incubated for 16 h at 4°C prior to the addition of selected amounts of super-shifting antibodies, anti-Purα 291 or anti-Purβ 302, to a final volume of 40 μL. After further 2 h incubation at 4°C, a total of 10 μL of each binding

reaction (typically 5,000 – 10,000 cpm) was loaded and resolved by non-denaturing electrophoresis as described in the main text.

Statistical Mechanical Analysis of Titration EMSA Data to Assess Cooperative Interactivity. Data points representing the fraction of each stoichiometric species observed by EMSA (Θ_0, Θ_1, and Θ_2) were fit to binding equations reflecting the relative probability of each possible configuration assuming two interacting binding sites on the DNA and a single protein (*7*).

$$\Theta_0 = \frac{1}{1 + (k_1 + k_2)[P_{free}] + k_1k_2k_c[P_{free}]^2} \qquad \text{(S7)}$$

$$\Theta_1 = \frac{(k_1 + k_2)[P_{free}]}{1 + (k_1 + k_2)[P_{free}] + k_1k_2k_c[P_{free}]^2} \qquad \text{(S8)}$$

$$\Theta_2 = \frac{(k_1k_2k_c)[P_{free}]^2}{1 + (k_1 + k_2)[P_{free}] + k_1k_2k_c[P_{free}]^2} \qquad \text{(S9)}$$

The microscopic constants k_1, k_2, and k_c only appear in two combinations in all three equations and can be replaced by substituting macroscopic constants $K_1 = k_1 + k_2$, and $K_2 = k_1k_2k_c$.(*7*). Thus, global fitting of species-specific isotherms resolves the macroscopic constants K_1 and K_2, from which microscopic constants can only be extracted in instances where there is no cooperativity or binding sites are identical.

Analysis of Serial-Dilution EMSA Data to Determination Purβ:PE32-F Stoichiometry. For the estimation of stoichiometry, a general cooperative binding mechanism $nP + D \rightleftarrows P_nD$ was assumed in which case the macroscopic association constant K_a is defined as:

$$K_a = [P_nD]/[P_{free}]^n[D_{free}] \qquad \text{(S10)}$$

where P represents N-HisPurβ, D represents PE32-F*, and n represents the stoichiometry of the nucleoprotein complex. Rearrangement of the definition of K_a gives an equation suitable for linear regression analysis.

$$\ln([P_nD]/[D_{free}]) = n\ln[P_{free}] + \ln K_a \qquad \text{(S11)}$$

Densitometric analysis of phosphorimages was done using ImageQuant 5.2 software (Molecular Dynamics) to determine $[P_nD]$ and $[D_{free}]$, whereas $[P_{free}]$ was estimated from the relationship:

$$[P_{free}] = [P_{input}] - n[P_nD] \qquad \text{(S12)}$$

where $[P_{input}]$ is the input concentration and n is an assigned integer value (1, 2, or 3) of the putative stoichiometry. Measured values of $[P_nD]$, $[D_{free}]$, and estimated values of $[P_{free}]$ were then used to calculate a value of n as the slope obtained from linear regression of a plot of $\ln([P_nD]/[D_{free}])$ versus $\ln[P_{free}]$). The assigned integer value of n was iteratively changed until the estimated and returned regression value of n converged. The value of $\ln K_a$ was also estimated from the intercept of the converged linear plot. Linear regression analyses were performed using Prism 5 software (GraphPad Software, Inc., San Diego, CA).

SUPPORTING RESULTS AND DISCUSSION

Analysis of N-HisPurβ Binding to Truncated Versions of the SMαA enhancer element. To map nucleotides required for specific, high affinity ssDNA-binding by N-HisPurβ, we designed and tested a panel of truncated oligonucleotides as competitors of N-HisPurβ interaction with PE32-bF by ELISA (Table S1). Figure S1 A and B show the competition curves generated using the –164 and –195 series, respectively. Nonlinear least-squares fitting of data points to equation 1 (main text) yielded IC_{50} values to estimate differences in apparent binding affinity. Self-competition by full-length PE32-F and its corresponding IC_{50} value was used as a reference point

for comparison to other oligonucleotides. As shown in Figure S1 C, deletions from either the 5′ or 3′ end of PE32-F reduced the apparent affinity for N-HisPurβ as signified by the progressively increasing IC_{50} values of the shorter competitors. A second series of oligonucleotides of fixed length (20 mer) that scan the entirety of PE32-F were also tested in the ELISA. As shown in Figure S2**,** oligonucleotides corresponding to the ends of PE32-F proved to be the most efficient competitors. These data suggested that the decreased affinity observed with deletion mutants was not solely explained by a reduction in lattice length, but rather, by elimination of specific nucleotide binding determinants near the 5′ and 3′ ends of PE32-F.

Comparison of Nucleoprotein Complexes Formed by Recombinant versus Non-Recombinant Purα/β. Figure S3 shows the band shift profiles of nucleoprotein complexes generated by equilibration of PE32-F* (1.0 nM) with purified N-HisPurβ, N-HisPurα, or crude AKR-2B fibroblast nuclear extract (N.E.). N-HisPurβ, at a concentration of 5.0 nM, shifts PE32-F* into two visible bands (lane 2), speculated to be N-HisPurβ_1:PE32-F* (lower band) and N-HisPurβ_2:PE32-F* (upper band). N-HisPurα at 5.0 nM (lane 7) produces a slightly slower migrating complex, which likely corresponds to N-HisPurα_2:PE32-F*. The subtle disparities in mobility of nucleoprotein complexes containing N-HisPurα or N-HisPurβ are consistent with known differences in the molecular weight and isoelectric point of each protein. Importantly, crude nuclear proteins from AKR-2B cells shift PE32-F* into a least two distinct complexes characterized by a lower band that runs similarly to the dominant N-HisPurβ complex, and an upper band, which runs similarly to the dominant N-HisPurα complex (lanes 4-6). Incubation of nuclear extract binding reactions with an antibody that specifically binds Purβ clearly identifies the lower band as a Purβ:PE32-F* complex, as indicated by its complete disappearance and the emergence of supershifted complexes, SS1 and SS2 (Figure S3, lanes 13 and 14). Conversely,

addition of an antibody that specifically binds Purα pointed to the upper band as a Purα:PE32-F* complex (lanes 15 and 16). The incomplete supershifting of this band may be a consequence of anti-Purα 291 possessing a lower affinity for its target complex than anti-Purβ 302. This supposition is supported by supershift profiles produced with recombinant Pur protein:ssDNA complexes (compare lanes 11 and 19). Taking into account small differences in the size and charge of the recombinant and naturally-occurring proteins, it is reasonable to infer from these data that the predominant, putative 2:1 protein:ssDNA complexes seen with N-HisPurβ and N-HisPurα mirror the complexes generated with Pur proteins synthesized by fibroblasts.

Monte Carlo error analysis of thermodynamic parameters. A lower level of experimental precision in DNase I footprint titrations translates in a higher level of uncertainty in fit parameters. As shown in the main text, free energy estimates from global fitting of individual site isotherms to a non-identical, two-site cooperative binding model carry with them relatively broad confidence intervals, especially in parameters that are cross-correlated by virtue of the mathematical expressions from which they are obtained. Estimated distributions for ΔG_1, ΔG_2, and ΔG_c in the context of the non-identical, interacting model were determined by Monte Carlo analysis simulating the experimentally observed level of error (± 13%), and obtaining fit parameters for each of 1000 iterations. The distributions of the returned parameters are depicted in Figure S5. The cross-correlation between ΔG_2 and ΔG_c can be readily seen by the mirror image, biphasic distributions of the two parameters, as well as their sheer broadness when error is simulated at ± 13%. The biphasicity persists until error is reduced to ± 5%, however, the width of the distributions remains significant for all levels of introduced error.

SUPPORTING REFERENCES

1. Ramsey, J. E., Daugherty, M. A., and Kelm, R. J., Jr. (2007) Hydrodynamic studies on the quaternary structure of recombinant mouse Purβ, *J. Biol. Chem. 282*, 1552-1560.
2. Knapp, A. M., Ramsey, J. E., Wang, S. X., Strauch, A. R., and Kelm, R. J., Jr. (2007) Structure-function analysis of mouse Purβ II. Conformation altering mutations disrupt single-stranded DNA and protein interactions crucial to smooth muscle alpha-actin gene repression, *J. Biol. Chem. 282*, 35899-35909.
3. Kelm, R. J., Jr., Elder, P. K., Strauch, A. R., and Getz, M. J. (1997) Sequence of cDNAs encoding components of vascular actin single-stranded DNA-binding factor 2 establish identity to Purα and Purβ, *J. Biol. Chem. 272*, 26726-26733.
4. Kelm, R. J., Jr., Cogan, J. J., Elder, P. K., Strauch, A. R., and Getz, M. J. (1999) Molecular interactions between single-stranded DNA-binding proteins associated with an essential MCAT element in the mouse smooth muscle α-actin promoter, *J. Biol. Chem. 274*, 14238-14245.
5. Lundblad, J. R., Laurance, M., and Goodman, R. H. (1996) Fluorescence polarization analysis of protein-DNA and protein-protein interactions, *Mol. Endocrinol .10*, 607-612.
6. Tretyachenko-Ladokhina, V., Ross, J. B., and Senear, D. F. (2002) Thermodynamics of E. coli cytidine repressor interactions with DNA: distinct modes of binding to different operators suggests a role in differential gene regulation, *J. Mol. Biol. 316*, 531-546.
7. Senear, D. F., and Brenowitz, M. (1991) Determination of binding constants for cooperative site-specific protein-DNA interactions using the gel mobility-shift assay, *J. Biol. Chem. 266*, 13661-13671.

Table S1. Sequences of deletion mutant oligonucleotides used as fluid-phase competitors in Purβ ssDNA-binding ELISA.

	Fluid Phase Competitor[a]	Sequence (5′ – 3′)
Truncation Series	PE32-F (-195/-164)[b]	GGGAGCAGAACAGAGGAATGCAGTGGAAGAGA
	-195/-166	GGGAGCAGAACAGAGGAATGCAGTGGAAGA
	-195/-168	GGGAGCAGAACAGAGGAATGCAGTGGAA
	-195/-170	GGGAGCAGAACAGAGGAATGCAGTGG
	-195/-172	GGGAGCAGAACAGAGGAATGCAGT
	-195/-174	GGGAGCAGAACAGAGGAATGCA
	-195/-176	GGGAGCAGAACAGAGGAATG
	-195/-178	GGGAGCAGAACAGAGGAA
	-195/-180	GGGAGCAGAACAGAGG
	-195/-182	GGGAGCAGAACAGA
	-195/-184	GGGAGCAGAACA
	-195/-186	GGGAGCAGAA
	-195/-188	GGGAGCAG
	-195/-190	GGGAGC
	-193/-164	GAGCAGAACAGAGGAATGCAGTGGAAGAGA
	-191/-164	GCAGAACAGAGGAATGCAGTGGAAGAGA
	-189/-164	AGAACAGAGGAATGCAGTGGAAGAGA
	-187/-164	AACAGAGGAATGCAGTGGAAGAGA
	-185/-164	CAGAGGAATGCAGTGGAAGAGA
	-183/-164	GAGGAATGCAGTGGAAGAGA
	-181/-164	GGAATGCAGTGGAAGAGA
	-179/-164	AATGCAGTGGAAGAGA
	-177/-164	TGCAGTGGAAGAGA
	-175/-164	CAGTGGAAGAGA
	-173/-164	GTGGAAGAGA
	-171/-164	GGAAGAGA
	-169/-164	AAGAGA
Scanning Series	PE32-F (-195/-164)[b]	GGGAGCAGAACAGAGGAATGCAGTGGAAGAGA
	-183/-164	GAGGAATGCAGTGGAAGAGA
	-185/-166	CAGAGGAATGCAGTGGAAGA
	-187/-168	AACAGAGGAATGCAGTGGAA
	-189/-170	AGAACAGAGGAATGCAGTGG
	-191/-172	GCAGAACAGAGGAATGCAGT
	-193/-174	GAGCAGAACAGAGGAATGCA
	-195/-176	GGGAGCAGAACAGAGGAATG

[a]Numbers indicate the position relative to transcription start site of the mouse SMαA gene.
[b]Full-length oligonucleotide used as self-competition control.

Table S2. Microscopic configurations and corresponding interaction free energy terms describing various models of two-site DNA-binding.

DNA Binding Models	Obligate Dimer		Identical Independent		Identical Interacting		Non-identical Independent		Non-identical Interacting	
Species Representation[1]	Free Energy Contribution[2]	Microscopic Constant	Free Energy Contribution[2]	Microscopic Constant	Free Energy Contribution[2]	Microscopic Constant	Free Energy Contribution[2]	Microscopic Constant	Free Energy Contribution[2]	Microscopic Constant
$s = 1$ 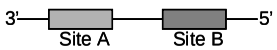	Reference state	-	Reference state	-	Reference state	-	Reference state	-	Reference state	-
$s = 2$ 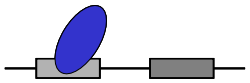 $n = 1$	-	-	ΔG_1	k_1	ΔG_1	k_1	ΔG_1	k_1	ΔG_1	k_1
$s = 3$ 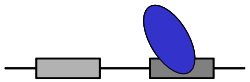 $n = 1$	-	-	ΔG_1	k_1	ΔG_1	k_1	ΔG_2	k_2	ΔG_2	k_2
$s = 4$ 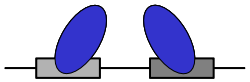 $n = 2$	-	-	$2\Delta G_1$	k_1^2	-	-	$\Delta G_1 + \Delta G_2$	$k_1 k_2$	-	-
$s = 5$ 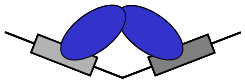 $n = 2$	$\Delta G_{di} + \Delta G_1$	$k_{di} k_1$	-	-	$2\Delta G_1 + \Delta G_c$	$k_1^2 k_c$	-	-	$\Delta G_1 + \Delta G_2 + \Delta G_c$	$k_1 k_2 k_c$

[1]Species diagrams represent possible microscopic configurations and do not necessarily reflect structural perturbations as a result of ligation, only that facilitation of binding occurs in the case of interacting sites. [2]Changes in free energy are related to microscopic constants by the equation $\Delta G_i = -RT\ln k_i$.

Table S3. Model-specific equations describing the fractional saturation of DNA sites A and B by protein based on a statistical mechanical method.

Hypothetical Model	Binding Equations
Obligate Dimer	$\bar{Y}_{A,B} = \frac{k_1 k_{di}[P_{free}]^2}{1 + k_1 k_{di}[P_{free}]^2}$
Identical, independent	$\bar{Y}_{A,B} = \frac{k_1[P_{free}] + k_1^2[P_{free}]^2}{1 + 2k_1[P_{free}] + k_1^2[P_{free}]^2}$
Identical, interacting	$\bar{Y}_{A,B} = \frac{k_1[P_{free}] + k_1^2 k_c[P_{free}]^2}{1 + 2k_1[P_{free}] + k_1^2 k_c[P_{free}]^2}$
Non-identical, independent	$\bar{Y}_A = \frac{k_1[P_{free}] + k_1 k_2[P_{free}]^2}{1 + (k_1 + k_2)[P_{free}] + k_1 k_2[P_{free}]^2}$ $\bar{Y}_B = \frac{k_2[P_{free}] + k_1 k_2[P_{free}]^2}{1 + (k_1 + k_2)[P_{free}] + k_1 k_2[P_{free}]^2}$
Non-identical, interacting	$\bar{Y}_A = \frac{k_1[P_{free}] + k_1 k_2 k_c[P_{free}]^2}{1 + (k_1 + k_2)[P_{free}] + k_1 k_2 k_c[P_{free}]^2}$ $\bar{Y}_B = \frac{k_2[P_{free}] + k_1 k_2 k_c[P_{free}]^2}{1 + (k_1 + k_2)[P_{free}] + k_1 k_2 k_c[P_{free}]^2}$

SUPPORTING FIGURE LEGENDS

FIGURE S1: Semi-quantitative analysis of N-HisPurβ interaction with deletion mutants of PE32-F. (A) and (B) Results of fluid-phase competitor titrations in an ELISA-based ssDNA-binding assay are shown for a panel of truncated oligonucleotides with a common 3′ (−164 series) or 5′ (−195 series) end. Points represent *mean* ± *s.d.* of measurements made in triplicate. Data points were fit to equation 1 (main text) to determine IC_{50} values for each competitor. (C) Resolved IC_{50} values are plotted for each fluid-phase competitor (best fit ± 67% confidence interval). Competitors marked with an asterisk indicate very low affinity as evidenced by a non-resolvable IC_{50} value.

FIGURE S2: Semi-quantitative analysis of N-HisPurβ interaction with scanning mutants of PE32-F. (A) Results of fluid-phase competitor titrations in an ELISA-based ssDNA-binding assay are shown for a series of 20mer oligonucleotides that scan PE32-F in two nucleotide increments. Points represent *mean* ± *s.d.* of measurements made in triplicate. Data points were fit to equation 1 (main text) to determine IC_{50} values for each competitor. (B) Resolved IC_{50} values are plotted for each fluid-phase competitor (best fit ± 67% confidence interval). Competitors marked with an asterisk indicate very low affinity as evidenced by a non-resolvable IC_{50} value.

FIGURE S3: Electrophoretic mobility (super)shift assay of purified, recombinant Purα and Purβ versus fibroblast-derived proteins. The relative electrophoretic mobilities of nucleoprotein complexes containing PE32-F* and either recombinant or nuclear extract-derived Purα or Purβ were compared in an attempt to identify the biologically relevant stoichiometric species. The predominant species observed with 5.0 nM N-HisPurβ and 1.0 nM PE32-F* (lane 2, predicted to be 2:1) is similar in mobility to the Purβ complex generated with nuclear extract (lanes 4-6). The

presence of Purβ in each complex was validated by supershifting with Purβ 302 antibody (compare lanes 10 and 11 to lanes 13 and 14). An analogous pattern is evident in N-HisPurα (lane 7) versus native Purα complexes (lanes 4-6). The presence of Purα in each complex was verified by supershifting with the Purα 291 antibody (compares lanes 18 and 19 to lanes 15 and 16). N.E., nuclear extract.

FIGURE S4: Statistical mechanical analysis of DNase I footprinting data to assess correspondence with conceptual models describing the interaction of N-HisPurβ with the MCAT-containing enhancer. Individual 3′ and 5′ site datasets were systematically and globally fit to equations describing various two-site models as illustrated in Tables S2 and S3. Blue symbols represent N-HisPurβ binding to the 3′ site. Red symbols represent binding to the 5′ site. Each point represents the *mean* ± *s.d.* of five independent experiments and the lines are best fit isotherms. Residual analysis and fit statistics best support a cooperative binding model involving two non-identical binding sites.

FIGURE S5: Monte Carlo error simulations to assess confidence in converged free energy values. Error-simulated individual site isotherms were globally fit to equations describing a two non-identical site, interacting model. Converged free energy parameters were plotted as frequency histograms of 1000 error simulations. Error levels of ±13% (the level experimentally observed) led to broad distributions of parameters ΔG_1 (black), ΔG_2 (light gray), and ΔG_c (dark gray). Systematically reducing the error from ±13% to ±5% restricts the distribution of $\Delta G1$, but not ΔG_2 or ΔG_c. The biphasic distributions of ΔG_2 and ΔG_c at all tested error levels are indicative of parameter cross-correlation.

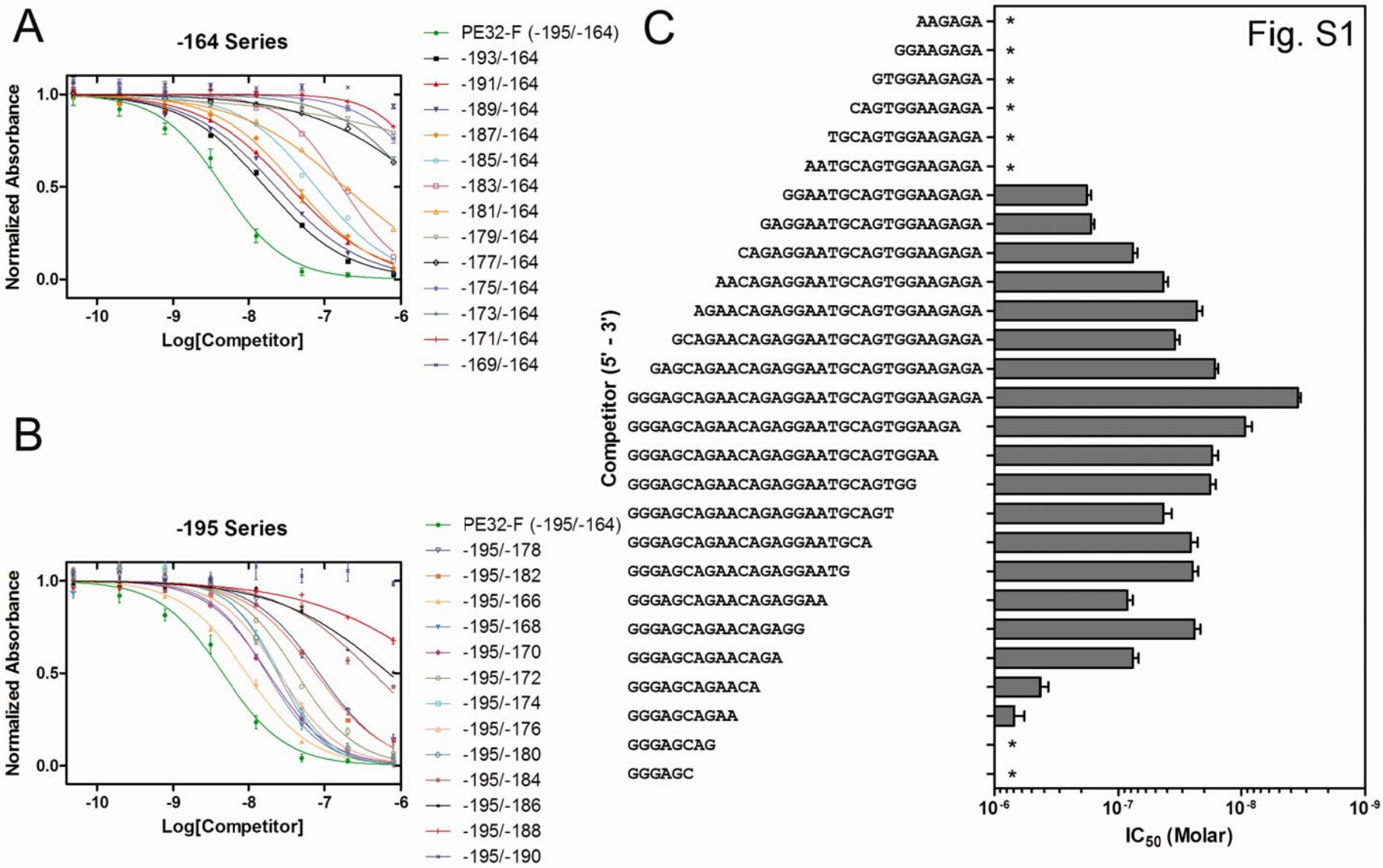
A
-164 Series
Normalized Absorbance
Log[Competitor]
PE32-F (-195/-164)
-193/-164
-191/-164
-189/-164
-187/-164
-185/-164
-183/-164
-181/-164
-179/-164
-177/-164
-175/-164
-173/-164
-171/-164
-169/-164
B
-195 Series
Normalized Absorbance
Log[Competitor]
PE32-F (-195/-164)
-195/-178
-195/-182
-195/-166
-195/-168
-195/-170
-195/-172
-195/-174
-195/-176
-195/-180
-195/-184
-195/-186
-195/-188
-195/-190
C
Fig. S1
Competitor (5' - 3')
AAGAGA
GGAAGAGA
GTGGAAGAGA
CAGTGGAAGAGA
TGCAGTGGAAGAGA
AATGCAGTGGAAGAGA
GGAATGCAGTGGAAGAGA
GAGGAATGCAGTGGAAGAGA
CAGAGGAATGCAGTGGAAGAGA
AACAGAGGAATGCAGTGGAAGAGA
AGAACAGAGGAATGCAGTGGAAGAGA
GCAGAACAGAGGAATGCAGTGGAAGAGA
GAGCAGAACAGAGGAATGCAGTGGAAGAGA
GGGAGCAGAACAGAGGAATGCAGTGGAAGAGA
GGGAGCAGAACAGAGGAATGCAGTGGAAGA
GGGAGCAGAACAGAGGAATGCAGTGGAA
GGGAGCAGAACAGAGGAATGCAGTGG
GGGAGCAGAACAGAGGAATGCAGT
GGGAGCAGAACAGAGGAATGCA
GGGAGCAGAACAGAGGAATG
GGGAGCAGAACAGAGGAA
GGGAGCAGAACAGAGG
GGGAGCAGAACAGA
GGGAGCAGAACA
GGGAGCAGAA
GGGAGCAG
GGGAGC
IC50 (Molar)

Fig. S2

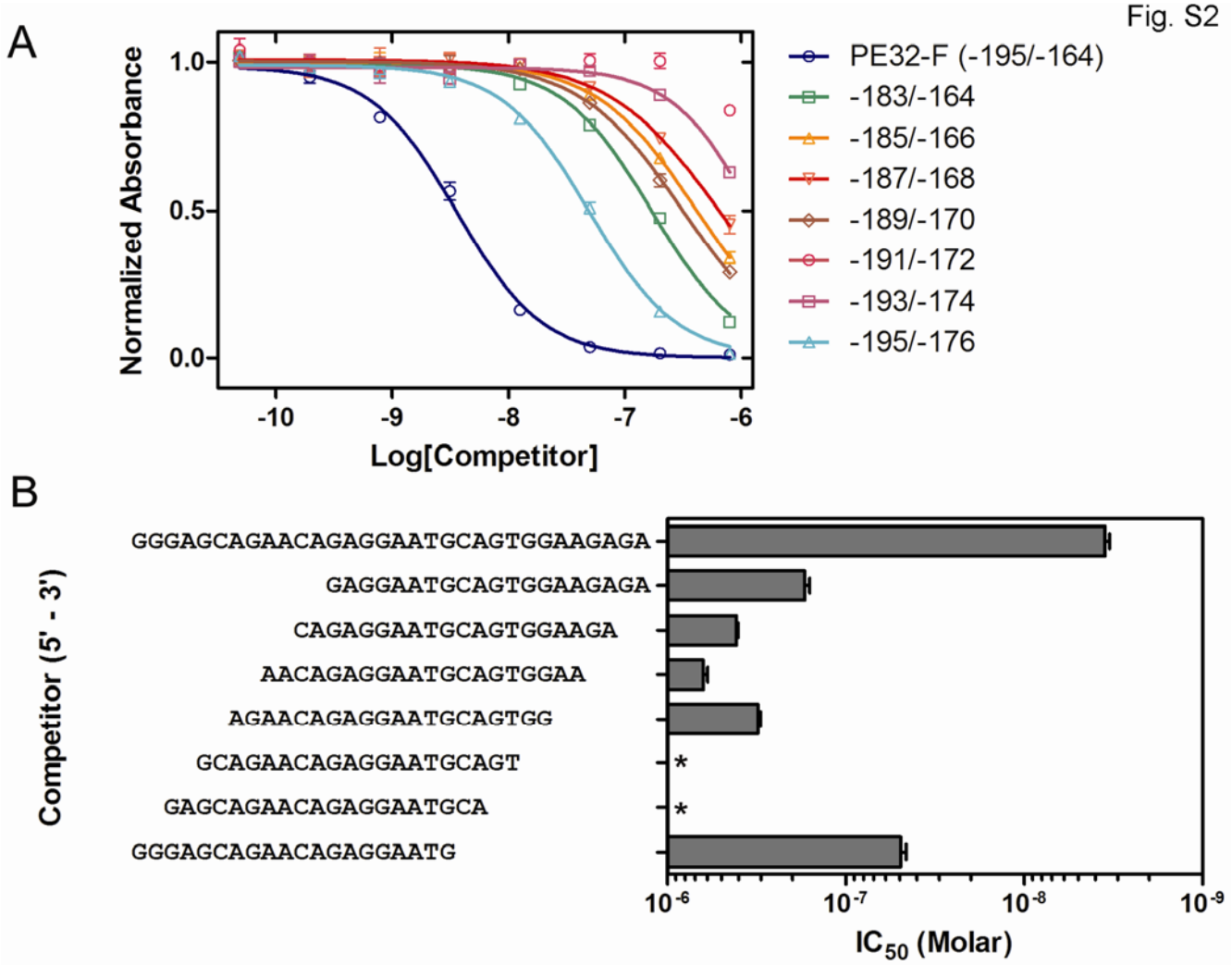
A
Normalized Absorbance
1.0
0.5
0.0
-10
-9
-8
-7
-6
Log[Competitor]
PE32-F (-195/-164)
-183/-164
-185/-166
-187/-168
-189/-170
-191/-172
-193/-174
-195/-176
B
Competitor (5' - 3')
GGGAGCAGAACAGAGGAATGCAGTGGAAGAGA
GAGGAATGCAGTGGAAGAGA
CAGAGGAATGCAGTGGAAGA
AACAGAGGAATGCAGTGGAA
AGAACAGAGGAATGCAGTGG
GCAGAACAGAGGAATGCAGT
GAGCAGAACAGAGGAATGCA
GGGAGCAGAACAGAGGAATG
*
*
10-6
10-7
10-8
10-9
IC50 (Molar)

Fig. S3

	1	2	3	4	5	6	7	8	9	10	11	12	13	14	15	16	17	18	19	20
5'-$^{32}PO_4$-PE32-F (nM)	1	1	1	1	1	1	1	1	1	1	1	1	1	1	1	1	1	1	1	1
N-HisPurβ (nM)	–	5	200	–	–	–	–	–	–	5	5	200	–	–	–	–	–	–	–	–
N-HisPurα (nM)	–	–	–	–	–	–	5	200	–	–	–	–	–	–	–	–	–	5	5	200
AKR-2B N.E. (μg/mL)	–	–	–	6.25	12.5	25	–	–	–	–	–	–	25	25	25	25	–	–	–	–
anti-Purβ 302 (μg/mL)	–	–	–	–	–	–	–	–	1	0.1	1	1	0.1	1	–	–	–	–	–	–
anti-Purα 291 (μg/mL)	–	–	–	–	–	–	–	–	–	–	–	–	–	–	0.1	1	1	0.1	1	1

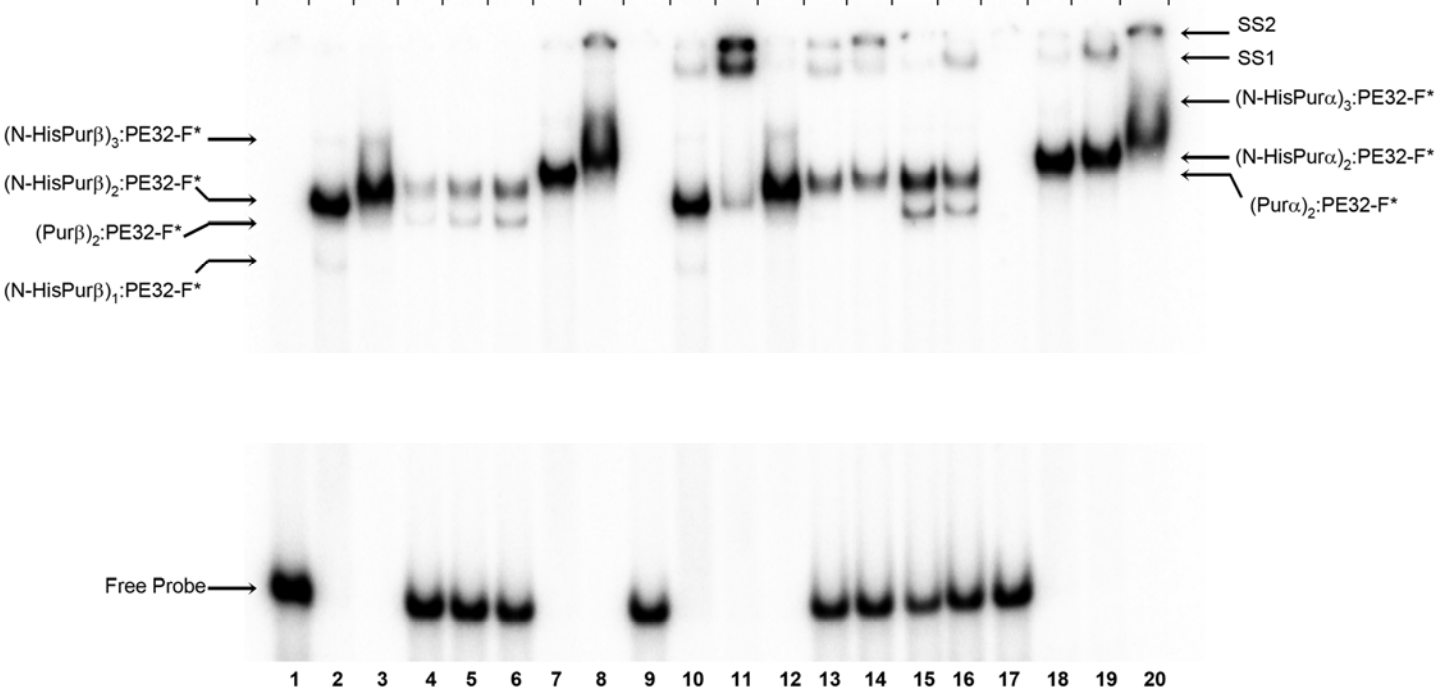

Fig. S4

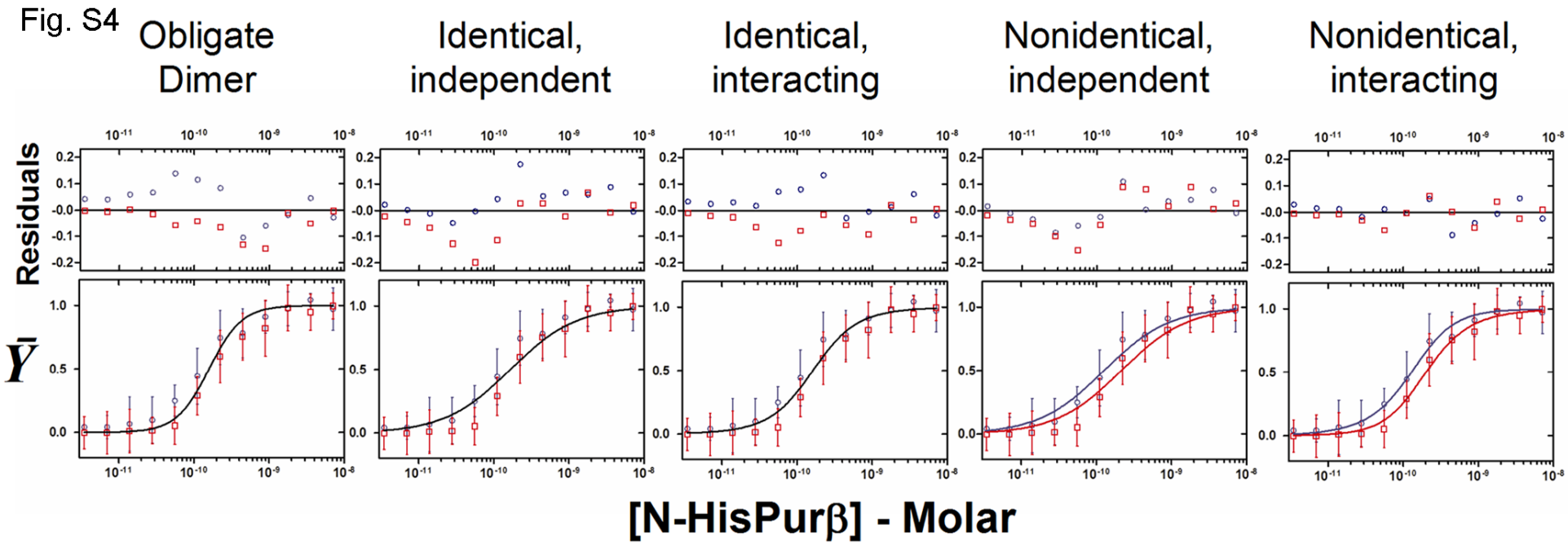
Obligate Dimer
Identical, independent
Identical, interacting
Nonidentical, independent
Nonidentical, interacting
Residuals
Ȳ
[N-HisPurβ] - Molar

Fig. S5

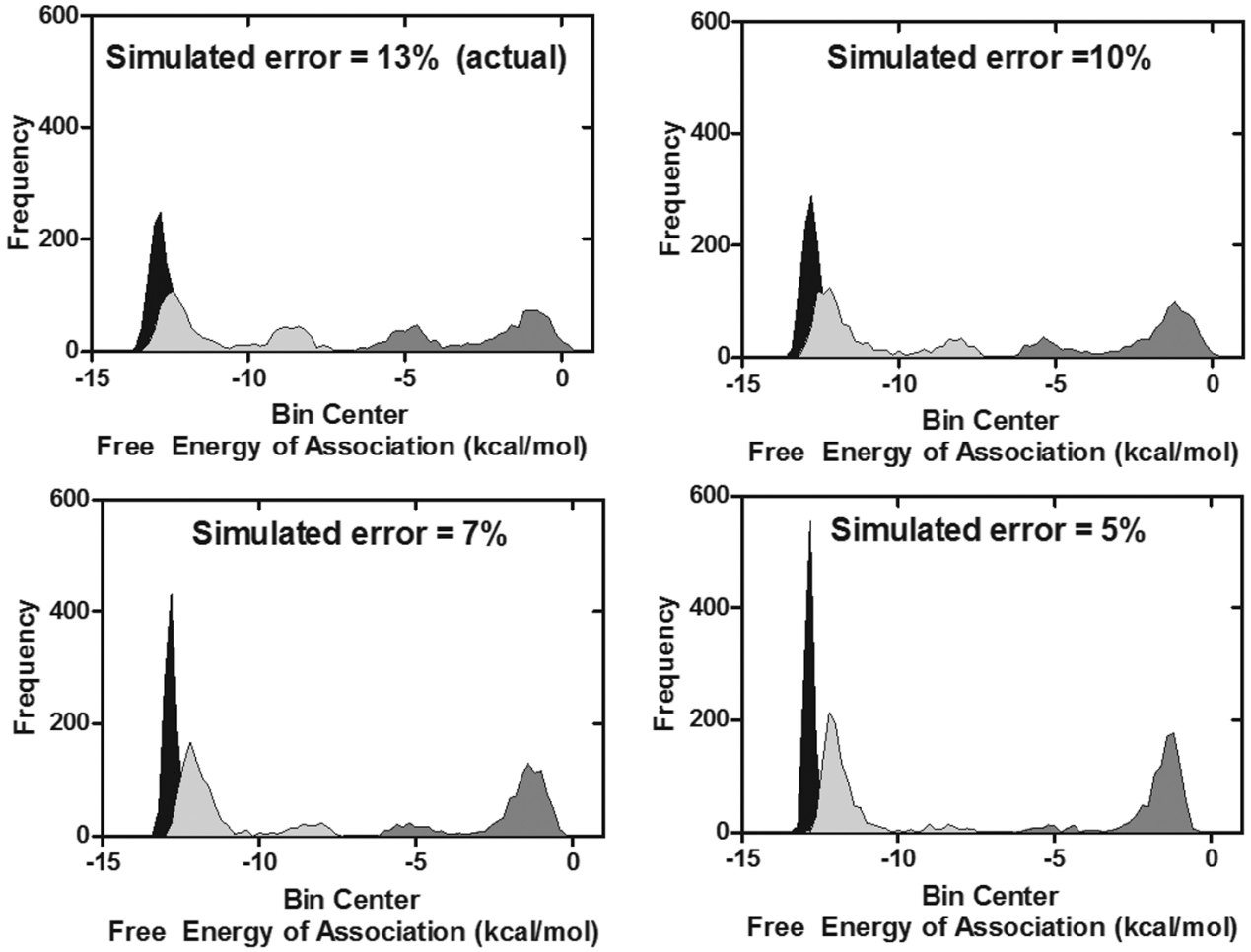
Simulated error = 13% (actual)
Simulated error =10%
Simulated error = 7%
Simulated error = 5%
Frequency
600
400
200
0
-15
-10
-5
0
Bin Center
Free Energy of Association (kcal/mol)